JOURNAL OF Materials CHEMISTRY

Solid-state reactions of vanadium(v) phosphates in the presence of ammonia

Andreas Martin,*[a] Ursula Steinike,[a] Klára Melánová[b] and Vítezslav Zima[b]

[a]*Institut für Angewandte Chemie Berlin-Adlershof e.V., Rudower Chaussee 5, D-12484 Berlin, Germany*
[b]*Joint Laboratory of Solid State Chemistry of the Academy of Sciences of the Czech Republic and University of Pardubice, Studenská 84, 532 10 Pardubice, Czech Republic*

Received 4th May 1999, Accepted 14th June 1999

The structural transformation of vanadyl(v) phosphate dihydrate ($V^{V}OPO_4{\cdot}2H_2O$, V/P = 1) and a Ga-containing vanadyl(v) phosphate dihydrate ($[Ga(H_2O)]_x(V^{V}O)_{1-x}PO_4{\cdot}2H_2O$, V/P = 1 − x) in the presence of ammonia have been investigated. $V^{V}OPO_4{\cdot}2H_2O$ was transformed in the presence of an NH_3–air–water vapour flow at temperatures of *ca.* 670 K mainly into distorted $(NH_4)_2(V^{IV}O)_3(P_2O_7)_2$ (V/P = 0.75). Additionally, the generation of crystalline V_2O_5 (up to 10%) was observed, mainly representing the remainder of the vanadium of the precursor compound. $[Ga(H_2O)]_x(V^{V}O)_{1-x}PO_4{\cdot}2H_2O$ was synthesised by the replacement of a number of the $(V^{V}O)^{3+}$ groups of the parent $V^{V}OPO_4{\cdot}2H_2O$ by $[Ga(H_2O)]^{3+}$. A similar solid-state transformation was observed when this material was treated under the same gas flow but, besides crystalline V_2O_5, a significant proportion of $GaPO_4$ was also formed. The heterogeneous catalytic ammoxidation of toluene to benzonitrile was applied as a test reaction in the temperature range 570–625 K for the evaluation of catalytic performance. The $V^{V}OPO_4{\cdot}2H_2O$ derived catalyst revealed an improved catalytic activity in comparison to similar catalysts obtained by the transformation of V(iv)-containing precursor compounds. It seems very likely that this is due to the existence of a proportion of crystalline V_2O_5. The catalytic activity of the Ga-containing material is much lower, but is still in the range of the V(iv)-derived catalysts. Characterisation of the parent samples and the generated products (after equilibration as well as catalytic runs) carried out by means of XRD, XPS and FTIR spectroscopy.

Vanadium phosphates (VPO) are well known as catalysts for the oxidation of *n*-butane to maleic anhydride (*e.g.* ref. 1 and references therein). Vanadyl(iv) pyrophosphate $(V^{IV}O)_2P_2O_7$ (V/P = 1) represents the outstanding material in this group of solids as it is considered to be the active and selective crystalline phase of such catalysts, mostly generated from $V^{IV}OHPO_4{\cdot}0.5H_2O$ *via* a topotactic transformation during activation (*e.g.* refs. 1–4) carried out under an inert gas. Besides $V^{IV}OHPO_4{\cdot}0.5H_2O$, that is mainly used as a catalyst precursor material, some related layered solids (*e.g.* $V^{V}OPO_4{\cdot}2H_2O$) are applied as catalysts. With the aim of obtaining a larger number of VPO materials to be applied as potential oxidation catalysts, a set of doped layered compounds of the general formula $[M^{III}(H_2O)]_x(V^{V}O)_{1-x}PO_4{\cdot}2H_2O$ (M^{III} = Al, Cr, Ga, Mn, Fe) has been prepared recently.[5–7]

In addition to their application as oxidation catalysts, VPO solids are also successfully employed as highly active and selective catalysts in the heterogeneous catalytic ammoxidation of toluene and substituted methyl aromatics and methyl heteroaromatics (*e.g.* refs. 8–12). The ammoxidation of these organic basic compounds to the corresponding nitriles is an industrially important reaction for the synthesis of several pharmaceuticals, dyestuffs and pesticides.

Recently, it was found by detailed *in situ* X-ray diffraction investigations, that in contrast to the generation of vanadyl(iv) pyrophosphate under an inert gas the precursor compound $V^{IV}OHPO_4{\cdot}0.5H_2O$ is transformed to an ammonium ion-containing solid $(NH_4)_2(V^{IV}O)_3(P_2O_7)_2$ under ammonia-containing gas flows in the temperature range *ca.* 573–673 K.[13] Additionally, the generation of an X-ray amorphous mixed-valence vanadium oxide phase (V_xO_y) was always evident as established by a variety of spectroscopic investigations. The V_xO_y phase accounts for the remainder of the vanadium content of the precursor compound since $(NH_4)_2(V^{IV}O)_3(P_2O_7)_2$ has a V/P ratio of 0.75 while the applied precursor compound has a V/P ratio of 1. Systematic investigations revealed the generation of similar $(NH_4)_2(V^{IV}O)_3(P_2O_7)_2$ catalysts from a variety of vanadyl(iv) hydrogenphosphates ($V^{IV}OHPO_4{\cdot}nH_2O$; n = 0, 2, 4; V/P = 1)[14–16] and vanadyl(iv) orthophosphates [$(V^{IV}O)_3(PO_4)_2{\cdot}nH_2O$; n = 7, 9; V/P = 1.5][17] under ammonia–air–water vapour flow at temperatures of *ca.* 670 K. Several years ago, initial investigations also indicated the potential of vanadyl(v) monophosphates as precursor compounds.[8]

The $(NH_4)_2(V^{IV}O)_3(P_2O_7)_2$ (AVP) materials generated by precursor transformation reactions are denoted in the following as AVP_{gen} whereas the pure as-synthesised solid is denoted AVP_{syn}. The AVP structure is isostructural to the K^+ salt, which is characterised by an orthorhombic structure (space group *Pnam*[18]) and an intersecting tunnel structure.[19,20] X-Ray investigations revealed a distorted AVP structure for the AVP_{gen} samples in comparison to that of the pure AVP_{syn} sample.[16] The two components of AVP_{gen} solids [$(NH_4)_2(V^{IV}O)_3(P_2O_7)_2$ and V_xO_y] do not form a simple mixture, but apparently form microdomains of AVP and V_xO_y which are intimately intergrown.[16,17]

The catalytic activity of the AVP_{gen} solids is obviously due to the generated vanadium oxide phase and it seems likely that the AVP structure probably simply acts as a matrix for the catalytically active V_xO_y phase, since AVP_{syn} itself is virtually catalytically inactive.[21] Moreover, it has recently been shown that the catalytic performance strongly depends on the precursor compound employed,[17] influencing the transformation process accompanied by varying concentrations of V_xO_y on the surface as well as varying the vanadium valence states of the V_xO_y phase.[17]

The purpose of the present study is to explore the phase transformations and evaluate of the catalytic performances of the formed AVP_{gen} catalysts in detail using pentavalent vanadium-containing precursor compounds such as pure

vanadyl(v) phosphate dihydrate $V^{V}OPO_4{\cdot}2H_2O$ (V/P = 1) and a Ga doped vanadyl(v) phosphate dihydrate. One fifth of the $(V^{V}O)^{3+}$ is replaced by $[Ga(H_2O)]^{3+}$ in the modified vanadyl(v) phosphate, allowing investigation of the influence of the introduced cation on the phase transformation and on the catalytic properties, which are mainly determined by the content, formation, valence state and accessibility of the V_xO_y phase. The catalytic results are compared to AVP_{syn} and an AVP_{gen} catalyst obtained using $V^{IV}OHPO_4{\cdot}0.5H_2O$ as precursor. The characterisation of the parent samples and the generated products (after equilibration as well as catalytic runs) was carried out by means of X-ray powder diffraction (XRD), X-ray photoelectron spectroscopy (XPS) and FTIR spectroscopy.

Experimental

Materials

$V^{V}OPO_4{\cdot}2H_2O$ (VP) was obtained by boiling a V_2O_5 suspension in aqueous phosphoric acid for 14 h.[22] A small amount of CrO_3 (0.1 g per 24 g of V_2O_5) was added to prevent any reduction of V^{V}. Subsequently, the reaction product was filtered off, washed with cold water and dried in air for three days at room temperature.

$[Ga(H_2O)]_{0.18}(V^{V}O)_{0.82}PO_4{\cdot}2H_2O$ (GaVP) was prepared by adding 24 g of V_2O_5 to a solution containing 160 ml of H_3PO_4 (85 mass%), 550 ml of distilled water and 24 g of $Ga(NO_3)_3{\cdot}9H_2O$. The reaction mixture was refluxed for 14 h and the suspension was hot filtered.[23] The resulting solid was washed with cold water and dried in air at room temperature.

$(NH_4)_2(V^{IV}O)_3(P_2O_7)_2$ (AVP_{syn}) and a $[(NH_4)_2(V^{IV}O)_3(P_2O_7)_2 + V_xO_y]$ solid (generated from $V^{IV}OHPO_4{\cdot}0.5H_2O$ and denoted $AVP_{gen0.5}$) were studied for comparison. The synthesis of pure AVP_{syn} was carried out by heating a mixture of 10 g of V_2O_5, 116 g of $(NH_4)_2HPO_4$ (0.88 mol) and a small amount of inoculating (seed) crystals at 598 K for 2.5 h in air.[15] $AVP_{gen0.5}$ was obtained by treatment of $V^{IV}OHPO_4{\cdot}0.5H_2O$ precursor under ammonia–air–water vapour (molar ratio = 1 : 7 : 5, total flow = 13 l h^{-1}) for 5 h at 673 K.[17] The precursor compound was synthesised according to the following procedure: 73 g of V_2O_5 were added to a hot mixture (353 K) of H_3PO_4 (85%, 1.04 mol) and 76 g of $(CO_2H)_2$ in 160 ml distilled H_2O under vigorous stirring for 18 h. The solution was cooled, filtered and the light-blue residue was dried overnight (423 K).[24]

Characterisation

The parent materials and the transformed as well as used samples were investigated by XRD. The patterns were recorded using a URD 6 (FPM-Seifert, Germany; reflection, Cu-Kα) and a STADI P (Stoe, Germany) set-up (transmission, Ge-primary-monochromator, Cu-Kα_1, capillary). Data interpretation was carried out using X-POW software (Stoe, Germany). The parent samples and the generated products were identified from the PDF-database (ICDD).

Surface analytical studies were performed using an ESCALAB 220iXL spectrometer (Fisons Instruments, Great Britain), consisting of two vacuum chambers: the analyser and a fast entry air lock/preparation chamber. The powdered samples were fixed on carbon tape (carbon conductive tape, Pelco International) at the top of the sample holder and transferred into an ultra-high vacuum. Monochromatic Al-Kα radiation (1486.6 eV) was applied as the X-ray source with an input power of 300 W. The emerging charge of the sample was equalised with installed charge compensation. Peak positions were calibrated using the C 1s peak (shifted to 285.0 eV) corresponding to absorbed carbon species. The XPS measurements were performed at a constant pass energy of 25 eV. The ESCALAB was calibrated routinely with the appropriate XPS lines of Au, Ag and Cu.[25] After background correction[26] the XPS spectra were recorded and the correct peak positions determined by Gaussian/Lorentzian peaks (with a tail function, if necessary, to take account of any asymmetry in the XPS signals of transition metal elements).[27] The sampling depth of these surface studies was estimated as *ca.* 7.5 nm by the mean free path of the electrons in the solid state.

The bulk V/P ratios were determined for single crystallites using a scanning electron microscope (ESEM 2020, Electroscan) equipped with an Si(Li)-detector for energy dispersive analysis of X-rays (EDX, Röntec).

IR spectra of the samples were recorded with a Perkin-Elmer System 2000 FTIR spectrophotometer using the KBr disk technique with *ca.* 1.5 mg of sample powder diluted in 300 mg of KBr and pressed into 20 mm od wafers. For each spectrum 10 scans were accumulated at 4 cm^{-1} resolution.

Chemical analyses (H, N) were carried out using an Elementar Analyzer 1110 (CE Instruments).

The surface areas of the catalytically employed materials were determined by N_2-physisorption using the BET method (Gemini III 2375, Micromeritics). The samples (*ca.* 0.5–1.0 g) were pretreated at 423–473 K for 1 h under vacuum.

Solid pretreatments and catalytic investigations

The precursor solids were heated under nitrogen flow (10 l h^{-1}) to *ca.* 393 K. Then the nitrogen was replaced by a flow (13.7 l h^{-1}) of ammonia–air–water vapour in the molar ratio 1 : 7.1 : 5.3. The samples were further heated at a rate of 10 K min^{-1} up to 673 K and kept for 5 h under these conditions to reach a steady state. After this equilibration procedure, the solids were cooled to room temperature under nitrogen. For a further pretreatment this procedure was repeated and the catalytic runs were carried out in a U-tube quartz-glass reactor (*ca.* 1.5 ml catalyst volume) under the following conditions: toluene : NH_3 : air : H_2O vapour = 1 : 4.5 : 32 : 24, atmospheric pressure, catalyst weight/volume flow (W/F) = 10 g h mol^{-1}, 673–723 K. Toluene conversion and benzonitrile formation were followed by on line-capillary GC (GC-17A, Shimadzu; column: FS-SE-54-CB, 25 m × 0.25 mm, Chrompak) using a flame-ionisation detector (FID). The total oxidation products (CO and CO_2) were determined by non-dispersive IR photometry (Infralyt 40E, Junkalor). The limit of detection of the carbon oxides was *ca.* 0.1 vol%. All materials used were pelletised (20 MPa, *ca.* 0.5 min), crushed and sieve fractions of 1.00–1.25 mm were applied for the catalytic runs. Table 1 summarises all materials used, treatment conditions and sample descriptions.

Results and discussion

Formation and characterisation of the solids

Fig. 1 shows XRD patterns of the parent materials used for the phase transformation investigations. The patterns of the as-synthesised solids were compared to data retrieved from the database of the International Centre for Diffraction Data (ICDD) (the relevant files are given in square brackets): it can be seen that VP [Fig. 1(a)] corresponds to $V^{V}OPO_4{\cdot}2H_2O$ [36-1472] [Fig. 1(b)] and GaVP [Fig. 1(c)] is isostructural to $[Mn(H_2O)]_{0.25}(V^{V}O)_{0.75}PO_4{\cdot}2H_2O$ [43-0778] [Fig. 1(d)].

XRD patterns of AVP_{syn} and the solid (AVP_{genVP}) generated during the pretreatment of the VP precursor are shown in Fig. 2(a) and (b), respectively. The main product of the AVP_{genVP} solid is a distorted AVP phase as shown in Fig. 2(b). It can be clearly seen that the crystallinity of AVP_{genVP} is poor in comparison to AVP_{syn}. One reason for this may be due to the formation of other crystalline solids, as discussed below, as well as the existence of X-ray amorphous material. Additionally, an

Table 1 Used materials, sample description and treatment conditions

Sample	Precursor compound	Treatment
VP_{pret1}	$V^{V}OPO_4{\cdot}2H_2O$	670 K, 5 h[a]
VP_{pret2}	$V^{V}OPO_4{\cdot}2H_2O$	670 K, 10 h[a]
AVP_{genVP}	$V^{V}OPO_4{\cdot}2H_2O$	670 K, 15 h[a] and catalytic runs[b]
$GaVP_{pret1}$	$[Ga(H_2O)]_{0.18}(V^{V}O)_{0.82}PO_4{\cdot}2H_2O$	670 K, 5 h[a]
$GaVP_{pret2}$	$[Ga(H_2O)]_{0.18}(V^{V}O)_{0.82}PO_4{\cdot}2H_2O$	670 K, 10 h[a]
$AVP_{genGaVP}$	$[Ga(H_2O)]_{0.18}(V^{V}O)_{0.82}PO_4{\cdot}2H_2O$	670 K, 15 h[a] and catalytic runs[b]

[a]Pretreatment: molar ratio of NH_3 : air : H_2O vapour = 1 : 7.1 : 5.3, heating rate = 10 K min^{-1}, 13.7 l h^{-1} total flow. [b]Catalytic runs: molar ratio of toluene : NH_3 : air : H_2O vapour = 1 : 4.5 : 32 : 24, atmospheric pressure, W/F = 10 g h mol^{-1}, 673–723 K.

increase of the *c*- and *b*-lattice parameters was observed in comparison to pure AVP_{syn}. Table 2 lists the unit cell parameters of both samples generated in this study in comparison to those of AVP_{syn}[18] and $AVP_{gen0.5}$.[17] AVP_{genVP} reveals a further increased deformation of the unit cell compared to $AVP_{gen0.5}$.

The generation of AVP_{genVP} from the precursor VP is already complete after the first pretreatment, *i.e.* the XRD patterns of the samples VP_{pret1}, VP_{pret2} and AVP_{genVP} are very similar. Crystalline V_2O_5 is always detected with increased intensity but along this series the improved detection after further pretreatment steps may be due to either increased content of V_2O_5 or of improved crystallinity. Approximately 10% V_2O_5 can be detected in AVP_{genVP} with the main peaks (*) at 4.38, 3.41, 2.88 Å. Furthermore, traces of $(V^{IV}O)_2P_2O_7$ (*ca.* 4%) were detected with main peaks (+) at 3.87, 3.14, 2.98 Å. By contrast, $AVP_{gen0.5}$ shows no evidence of containing crystalline solids other then AVP.

The precursor sample VP (V/P = 1) is transformed into AVP_{genVP} which contains 75% of the original vanadium in the crystalline AVP phase (V/P = 0.75) owing to stoichiometric considerations.[17] The remainder of the vanadium could occur in the form of crystalline co-phases and rather more likely as X-ray amorphous vanadium oxides or vanadium phosphates. Surprisingly, in the case of the VP transformation, a proportion of this remainder forms crystalline phases [V_2O_5 and traces of $(V^{IV}O)_2P_2O_7$], this being observed for the first time during such transformations. Furthermore, X-ray amorphous vanadium-containing compounds could exist, probably being of mixed-valence, since ammonia can act as a reducing agent. The formation of such X-ray amorphous vanadium oxide phases from the excess vanadium is also known from other phase transformations[16,17] and a detailed discussion on the distribution of vanadium is described in ref. 17.

XRD patterns of AVP_{syn}, $GaVP_{pret1}$ and $AVP_{genGaVP}$ are shown in Fig. 3(a), (b) and (c), respectively. The onset of the generation of AVP was observed after the first pretreatment (with the main peaks (′) at 5.595, 3.70 Å) as well as peaks of $V^{V}OPO_4$ and $GaPO_4$. The formation of AVP from this modified sample is delayed in comparison to the formation of AVP_{genVP}, and the solid obtained after the repeated treatment procedure ($AVP_{genGaVP}$) consists of *ca.* 60% of a deformed AVP (see also Table 2). Furthermore, several additional crystalline phases can be detected: $GaPO_4$ (*ca.* 30%) with main peaks (#) at 4.00, 2.82, 2.46, 3.11 Å and small

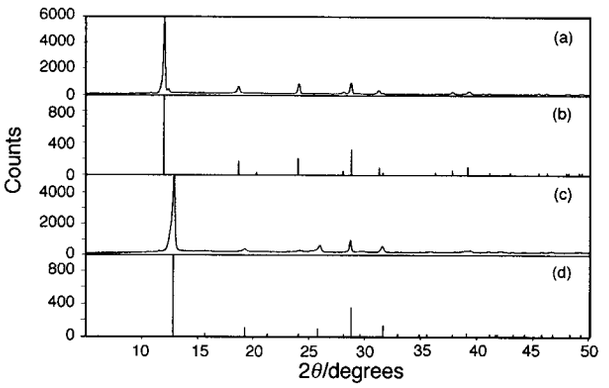

Fig. 1 XRD patterns of as-synthesised parent materials: (a) $V^{V}OPO_4{\cdot}2H_2O$ (VP), (b) $V^{V}OPO_4{\cdot}2H_2O$ [36-1472] for comparison, (c) $[Ga(H_2O)]_{0.18}(V^{V}O)_{0.82}PO_4{\cdot}2H_2O$ (GaVP) and (d) $[Mn(H_2O)]_{0.25}(V^{V}O)_{0.75}PO_4{\cdot}2H_2O$ [43-0778] for comparison.

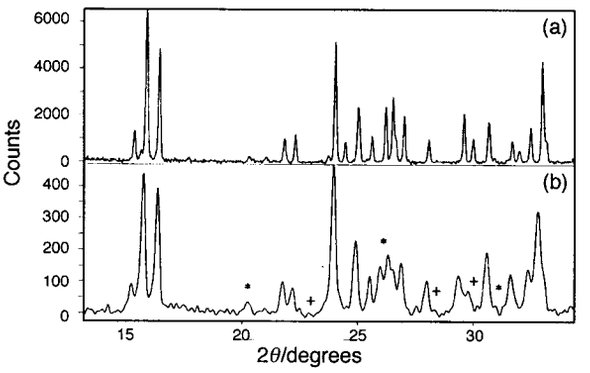

Fig. 2 XRD patterns of as-synthesised, pure $(NH_4)_2(V^{IV}O)_3(P_2O_7)_2$ (AVP_{syn}) (a), the solid generated from $V^{V}OPO_4{\cdot}2H_2O$ (VP) phase transformation after pretreatment and catalytic runs denoted as AVP_{genVP} (b), showing additional proportions of V_2O_5 (*[41-1426]) and $(V^{IV}O)_2P_2O_7$ (+[34-1381]).

Table 2 Unit cell parameters of as-synthesised, pure $(NH_4)_2(V^{IV}O)_3(P_2O_7)_2$ (AVP_{syn}),[27] $AVP_{gen0.5}$ from $V^{IV}OHPO_4{\cdot}0.5H_2O$,[17] AVP_{genVP} from $V^{V}OPO_4{\cdot}2H_2O$ and $AVP_{genGaVP}$ generated from $[Ga(H_2O)]_{0.18}(V^{V}O)_{0.82}PO_4{\cdot}2H_2O$

Sample	*a*/Å	*b*/Å	*c*/Å	*V*/Å^3
AVP_{syn}	17.498	11.365	7.277	1447.14
$AVP_{gen0.5}$	17.504	11.381	7.329	1460.03
AVP_{genVP}	17.501	11.390	7.348	1465.25
$AVP_{genGaVP}$	17.507	11.385	7.329	1459.02

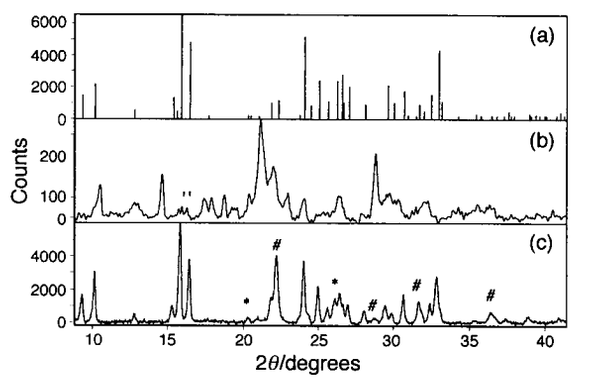

Fig. 3 XRD patterns of as-synthesised, pure $(NH_4)_2(V^{IV}O)_3(P_2O_7)_2$ (AVP_{syn} [47-804]) (a), the solid generated from $[Ga(H_2O)]_{0.18}(V^{V}O)_{0.82}PO_4{\cdot}2H_2O$ (GaVP) phase transformation after the first pretreatment (molar ratio: NH_3 : air : H_2O : vapour = 1 : 7.1 : 5.3, 670 K, 5 h) denoted as $GaVP_{pret1}$ (b) and the solid obtained after pretreatment and catalytic runs denoted as $AVP_{genGaVP}$ (c) (the symbols indicate different phases: (′) AVP_{syn} [47-804], (#) $GaPO_4$ [31-546] and (*) V_2O_5 [41-1426]).

Table 3 Chemical analyses, BET surface areas and bulk V/P ratio *vs.* surface V/P ratio of AVP_{syn} and generated AVP specimens

Sample	H/N molar ratio	BET surface area/m^2 g^{-1}	V/P (bulk)[a]	V/P (surf.)[b]
AVP_{syn}	4.0	5.00	0.75	0.33
$AVP_{gen0.5}$[17]	3.6	2.95	1.00	1.00
AVP_{genVP}	3.4	3.36	1.00	1.00
$AVP_{genGaVP}$	3.1	4.58	n.d.	1.30 (Ga≫V)[c]

[a]Measured by energy dispersive analysis of X-rays (EDX).[16] [b]Measured by XPS. [c](V+Ga)/P(surf.).

Table 4 Catalytic performance of AVP_{genVP} from $V^{V}OPO_4{\cdot}2H_2O$ and $AVP_{genGaVP}$ from $[Ga(H_2O)]_{0.18}(V^{V}O)_{0.82}PO_4{\cdot}2H_2O$ samples during ammoxidation of toluene (X_{tol} = toluene conversion, Y_{bn} = benzonitrile yield and Y_{CO_x} = CO + CO_2 yield)

Sample	T/K	X_{tol} (mol%)	Y_{bn} (mol%)	Y_{CO_x}(mol%)
AVP_{genVP}	575	1.8	1.7	<0.1
	600	7.1	6.3	0.8
	625	18.7	16.9	1.8
$AVP_{genGaVP}$	575	1.8	1.7	<0.1
	600	5.2	4.7	0.4
	625	13.3	12.2	0.9

amounts of crystalline V_2O_5 with main peaks (*) at 4.38, 3.41, 2.88 Å.

Additionally, it was observed during *in situ*-XRD measurements[13] of the GaVP transformation under the conditions of the ammoxidation reaction at 670 K, that $GaPO_4$ is transformed from the hexagonal form ($GaPO_4$ [8-497], observed also in $GaVP_{pret1}$) to the cubic form ($GaPO_4$ [31-547]). This corresponds to the transformation of the low-temperature quartz-type modification of $GaPO_4$ to the high-temperature cristobalite-type modification of $GaPO_4$. A similar transformation of $GaPO_4$ is described in the literature[28,29] but is observed at significantly higher temperatures (1200 K) under air. $GaPO_4$ is transformed during cooling (observed by *in situ*-XRD) from the high-temperature cristobalite-type modification that is present during the reaction conditions of the ammoxidation into the orthorhombic low-temperature cristobalite-type modification ($GaPO_4$ [31-546]).[13]

The FTIR spectra of the generated AVP_{genVP} and $AVP_{genGaVP}$ solids reveal a similar appearance to that of the as-synthesized AVP_{syn} and of $AVP_{gen0.5}$ (Fig. 4). The spectra of the generated specimens reveal less sharp and resolved bands compared to AVP_{syn} owing to their decreased crystallinity and probable increased amount of amorphous material as well as of crystalline co-phases. Assignment of various bands in the region 970–1010 region (V=O vibrations) to discrete V=O species can only be speculative; ref. 17 outlines the problematic nature of IR band assignment in VPO solids.

Table 3 reports chemical analyses data, BET surface areas and bulk V/P ratios as well as surface V/P ratios of various AVP solids. XPS investigations revealed the V/P ratios on the surface and EDX studies those of the bulk of the AVP_{genVP} and $AVP_{genGaVP}$ solids compared with AVP_{syn} and $AVP_{gen0.5}$. The results are similar to data published recently: AVP_{syn} shows an enrichment of phosphorus on the solid surface in comparison to the bulk. XPS analyses of AVP_{genVP} and $AVP_{gen0.5}$ revealed the same V/P ratio on the surface as observed for the bulk V/P ratio determined by EDX. The higher V/P_{surf} ratio of AVP_{gen} solids compared with AVP_{syn} is due to the existence of V_xO_y phases on the sample surface. The additional V_xO_y might compensate for the expected phosphorus surplus on the surface of AVP_{syn}. Additionally, a surplus of Ga on the surface was found for $AVP_{genGaVP}$.

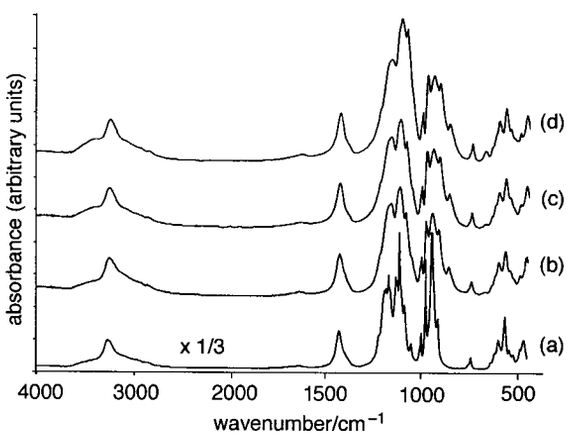

Fig. 4 FTIR spectra of as-synthesised, pure $(NH_4)_2(V^{IV}O)_3(P_2O_7)_2$ (AVP_{syn}) (a) and samples obtained by phase transformations: (b) $AVP_{gen0.5}$, (c) AVP_{genVP} and (d) $AVP_{genGaVP}$.

Catalytic investigations

The catalytic performances of the AVP_{genVP} and $AVP_{genGaVP}$ specimens were measured for the ammoxidation of toluene to benzonitrile (Table 4). As expected, the catalytic activity is increased with increased reaction temperature and benzonitrile selectivities >90% are the rule. The catalytic activity of AVP_{genVP} is higher than that of $AVP_{genGaVP}$. This ranking is also mirrored in area-specific rates of toluene conversion (R_{tol}/μmol h^{-1} m^{-2}) as shown in Fig. 5 which also includes, for comparison, known activity data for AVP_{syn} and $AVP_{gen0.5}$ catalysts observed for similar reaction conditions.

As described in detail recently,[17] the reason for the catalytic activity of the generated AVP_{gen} catalysts is the existence of additional vanadium oxides on the catalyst surface. Highly crystalline AVP_{syn} is fairly catalytically inactive and it appears likely to only act as a support or matrix for the generated vanadium oxides in the AVP_{gen} samples. The AVP_{genVP} sample reveals the highest conversion rate; one reason for its higher catalytic activity in comparison to $AVP_{gen0.5}$ could be attributed to the existence of a readily detectable crystalline V_2O_5 phase, which could be due to the fact that a V(v) compound was used as the precursor in comparison to the use of $V^{IV}OHPO_4{\cdot}0.5H_2O$ for the generation of the $AVP_{gen0.5}$ sample. Crystalline V_2O_5 is probably more readily formed during the phase transformation from the V(v) precursor. In contrast, it seems likely that the generation of a crystalline V(v)-containing phase using a V(iv) precursor as the parent sample under the reducing ammonia atmosphere is much more difficult. $AVP_{genGaVP}$ shows a significantly lower rate of toluene conversion, reflecting the decreased proportion of

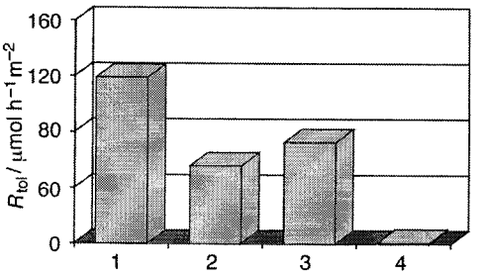

Fig. 5 Catalytic activity (R_{tol}/μmol_{tol} h^{-1} m^{-2}, area-specific rate of toluene conversion) of several generated catalyst specimens compared to AVP_{syn} in the ammoxidation of toluene to benzonitrile at 620 K (1, AVP_{genVP}; 2, $AVP_{genGaVP}$; 3, $AVP_{gen0.5}$ and 4, AVP_{syn}).

surface vanadium oxide species, however crystalline V_2O_5 is observed.

Conclusions

The investigations have shown that both pentavalent vanadium-containing VPO solids ($V^{V}OPO_4{\cdot}2H_2O$ and $[Ga(H_2O)]_{0.18}(V^{V}O)_{0.82}PO_4{\cdot}2H_2O$) can be transformed into ammonium vanadyl pyrophosphates under an NH_3–air–water vapour flow at temperatures of *ca.* 670 K. The phase transformation of $V^{V}OPO_4{\cdot}2H_2O$ leads to a detectable amount of crystalline V_2O_5 besides smaller amounts of crystalline $(V^{IV}O)_2P_2O_7$. The transformation of $[Ga(H_2O)]_{0.18}(V^{V}O)_{0.82}PO_4{\cdot}2H_2O$ also reveals the formation of crystalline V_2O_5 along with an enrichment of Ga on the solid surface accompanied with the formation of $GaPO_4$. The $V^{V}OPO_4{\cdot}2H_2O$ derived sample shows the highest catalytic activity in comparison to materials based on V(IV)-containing precursor compounds owing to the existence of crystalline V_2O_5. Furthermore, modifications of the $(NH_4)_2(V^{IV}O)_3(P_2O_7)_2$ structure could also play an important role in the catalytic cycle.

Acknowledgements

The authors thank Dr P. Druska for the XPS investigations and Mrs I. Rau and Mrs H. French for experimental assistance. This work was supported by the Federal Ministry of Education and Research, Germany and the Senate of Berlin (project No. 03C3005) and by the Fonds der Chemischen Industrie.

References

1 E. Bordes, *Catal. Today*, 1987, **1**, 499.
2 G. Hutchings, *Appl. Catal.*, 1991, **72**, 1.
3 *Vanadyl Pyrophosphate Catalysts*, ed. G. Centi, *Catal. Today*, 1993, **16**(1).
4 C. C. Torardi, Z. G. Li, H. S. Horowitz, W. Liang and M. H. Whangbo, *J. Solid State Chem.*, 1995, **119**, 349.
5 L. Beneš, P. Galli, M. A. Massucci, K. Melánová, P. Patrono and V. Zima, *J. Therm. Anal.*, 1997, **50**, 355.
6 K. Richtrová, J. Votinský, J. Kalousová, L. Beneš and V. Zima, *J. Solid State Chem.*, 1995, **116**, 400.
7 G. Bagnasco, L. Beneš, P. Galli, M. A. Massucci, P. Patrono, M. Turco and V. Zima, *J. Therm. Anal.*, 1998, **52**, 615.
8 A. Martin, B. Lücke, H. Seeboth, G. Ladwig and E. Fischer, *React. Kinet. Catal. Lett.*, 1989, **38**, 33.
9 A. Martin, B. Lücke, H. Seeboth and G. Ladwig, *Appl. Catal.*, 1989, **49**, 205.
10 I. Matsuura, *Stud. Surf. Sci. Catal.*, 1992, **72**, 247.
11 A. Martin, H. Berndt, B. Lücke and M. Meisel, *Top. Catal.*, 1996, **3**, 377.
12 A. Martin and B. Lücke, *Catal. Today*, 1996, **32**, 279.
13 L. Wilde, unpublished results.
14 Y. Zhang, M. Meisel, A. Martin, B. Lücke, K. Witke and K.-W. Brzezinka, *Chem. Mater.*, 1997, **9**, 1086.
15 Y. Zhang, A. Martin, G.-U. Wolf, S. Rabe, H. Worzala, B. Lücke, M. Meisel and K. Witke, *Chem. Mater.*, 1996, **8**, 1135.
16 U. Steinike, F. Krumeich, L. Wilde, A. Martin, and G.-U. Wolf, *Mater. Sci. Forum*, 1998, **278–281**, 660 (ISBN: 0-87849-807-9).
17 A. Martin, G.-U. Wolf, U. Steinike and B Lücke, *J. Chem. Soc., Faraday Trans.*, 1998, **94**, 2227.
18 J. Trommer, H. Worzala, S. Rabe and M. Schneider, *J. Solid State Chem.*, 1998, **136**, 181.
19 A. Leclaire, H. Chahboun, D. Groult and B. Raveau, *J. Solid State Chem.*, 1988, **77**, 170.
20 K. H. Lii, Y. P. Wang and S. L. Wang, *J. Solid State Chem.*, 1989, **80**, 127.
21 A. Martin, A. Brückner, Y. Zhang and B. Lücke, *Stud. Surf. Sci. Catal.*, 1997, **108**, 377.
22 G. Ladwig, *Z. Anorg. Allg. Chem.*, 1965, **338**, 266.
23 K. Melánová, J. Votinský, L. Beneš and V. Zima, *Mater. Res. Bull.*, 1995, **30**, 1115.
24 H. Berndt, K. Büker, A. Martin, M. Meisel, A. Brückner and B. Lücke, *J. Chem. Soc., Faraday Trans.*, 1995, **91**, 725.
25 M. T. Anthony and M. P. Seah, *Surf. Interface Anal.*, 1984, **6**, 95.
26 D. A. Shirley, *Phys. Rev. B: Condens. Matter*, 1972, **5**, 4709.
27 R. O. Ansell, T. Dickinson, A. F. Povey and P. A. M. Sherwood, *J. Electroanal. Chem.*, 1979, **98**, 79.
28 O. Baumgärtner, A. Preisinger, P. W. Krempl and H. Mang, *Z. Kristallogr.*, 1984, **168**, 83.
29 H. Sowa, *Z. Kristallogr.*, 1994, **209**, 954.

Paper 9/03491I